Multifractal analysis of tori destruction in a molecular Hamiltonian system

A. M. Tarquis
Departamento de Matemática Aplicada, Escuela Técnica Superior de Ingenieros Agrónomos, Universidad Politécnica de Madrid, 28040 Madrid, Spain

J. C. Losada and R. M. Benito*
Departamento de Física y Mecánica, Escuela Técnica Superior de Ingenieros Agrónomos, Universidad Politécnica de Madrid, 28040 Madrid, Spain

F. Borondo†
Departamento de Química, C–IX, Universidad Autónoma de Madrid, Cantoblanco 28049 Madrid, Spain
(Received 2 August 2001; published 20 December 2001)

In this paper, an analysis of the phase space structure of the isomerizing molecular system LiNC/LiCN, using Poincaré surfaces of section and frequency analysis, is presented. The scaling structure of the frequency map in the chaotic region next to the regular part corresponding to the stable linear isomer LiNC is studied using multifractal analysis. This approach is a way to characterize quantitatively the complexity in the mechanism of the tori destruction in a molecular Hamiltonian system that exhibits soft chaos as the vibrational energy of the system increases.

DOI: 10.1103/PhysRevE.65.016213 PACS number(s): 05.45.Ac, 05.45.Df, 05.45.Tp

I. INTRODUCTION

From the vibrational point of view, molecules can be considered as Hamiltonian systems formed by a collection of nonlinear anharmonic coupled oscillators. The corresponding classical dynamics can be interpreted in terms of phase space structures that, although envisaged by Poincaré at the end of the nineteenth century, could only be properly studied after the development of modern digital computers [1]. For low levels of excitations molecular motions take place in the vicinity of the minima of the potential energy surface, defined within the Born-Oppenheimer approximation. In this harmonic regime the motion is regular, corresponding to the well known normal mode picture [2]. The combination of anharmonicities and strong mode couplings, as vibrational energy increases, makes molecules nonintegrable dynamical systems, with the possibility of undergoing chaotic motion [3]. The celebrated Kolmogorov-Arnold-Moser (KAM) theorem provides a very powerful framework to understand this transition to chaos. When some perturbation acts on an integrable system some tori are destroyed, but those with ''irrational enough'' frequency ratios (in the sense of the KAM condition), called KAM tori, survive [4]. In two-degrees-of-freedom (2dof) systems, these structures establish a hierarchical organization of phase space. The family of persistent KAM tori, parametrized by a Cantor set of frequency vectors in the ''holes'' of which chaotic behavior takes place, constitutes an impenetrable barrier for the flux of trajectories across. The destroyed tori turn into periodic orbits (PO), homoclinic tangles, and cantori [3]. Periodic orbits correspond to resonant motion (rational frequency ratio) and are organized in phase space according to a Farey tree distribution [5]. Emanating from each unstable PO fixed point there are two associated manifolds, one incoming and another outgoing, whose repeated crossings form the homoclinic tangle: a band of stochasticity that can be tiled, classifying the different regions according to their dynamical properties [1]. Cantori are fractal objects [6], originated by the destruction of the ''not irrational enough'' tori in the unperturbed system; that act as partial barriers in the chaotic regions of phase space. As perturbation increases, the fractal dimension of these structures decreases, and the corresponding barrier effect weakens [7]; at the same time more and more KAM tori enter into this category. Then, the dynamical bottleneck in a given phase space region corresponds to the most intact cantori, i.e., the last broken KAM torus corresponding to that with the most irrational frequency ratio. According to the continued fraction theory [8], this corresponds to the golden mean, defined as

$$\gamma = 1 + \cfrac{1}{1 + \cfrac{1}{1 + \cdots}} = \frac{1+\sqrt{5}}{2}. \tag{1}$$

The destruction of tori has been systematically studied in the standard map [3] by a number of authors [9], and some fractal structures in the diagrams of the breakup of tori had been identified by Schmidt and Bialek [10].

There are numerous methods to investigate the structure of phase space. In systems with a 2dof composite Poincaré surface of section (SOS), consisting of the intersection of the trajectories at a given energy with suitable surfaces, there is more informative than other tools [11], such as Lyapunov exponents or Kolmogorov entropy. Unfortunately, a SOS is not feasible for systems with more than 2dof.

An alternative method is that of frequency analysis (FA), which is based on a Fourier representation of trajectories. The FA method involves monitoring the variations of the fundamental frequencies of the system with time. In the case of regular motion, an analytical representation for the solution of the Hamilton equations of motion is obtained,

*Electronic mail: rbenito@fis.etsia.upm.es
†Electronic mail: f.borondo@uam.es

whereas when the dynamics are chaotic the expansion does not converge. However, FA is still able to provide some information of the local (short time dynamics) characteristics of the chaotic motion. The advantage of this method is that it can be applied equally easily to systems with more than 2dof [12], so that is suitable to study the poorly understood Arnold web [13].

In a previous paper [14] we used the FA, as implemented by Laskar [15] in his analysis of the stability of the solar system [16], to study the phase space structure and local behavior of chaotic trajectories of a complex molecular isomerizing system: the LiNC/LiCN molecule. One of the most interesting conclusions of the paper was to reveal that, contrary to what could be expected *a priori*, the chaotic region for energies in the range 2950–3850 cm^{-1} was extremely influenced by a single PO, in which the stretching Li-CN and the bending motions were coupled by a 1:8 (frequency) resonance. Frequency maps provide very useful information on the way in which the trajectories evolve in phase space.

The aim of this paper is to study in deeper detail the characteristics of the chaotic region, especially its border near the regular one, in this molecular system. As it is well known, the coexistence of the different types of dynamical structures that we have just described impose a fractal structure, self-similar at different scales, into the phase space in which they are embedded. For this purpose, we will carry out a multifractal analysis (MFA) [17] of the frequency map consisting of the frequency ratio vs the initial bending angle representation. Furthermore, by considering the results obtained at different values of the excitation energy, we can follow the process of destruction of KAM tori.

Other complex processes occurring in nature, such as turbulence [18], large-scale structure formation [19], particle size distribution in soils [20] or diffusion-limited aggregation [21], to name just a few, are also believed to be organized in a self-similar or self-affine way. Statistical self-similar measures arise naturally in phenomena associated with nonlinear or chaotic systems. A convenient tool to characterize the configurations of these processes is also MFA [22,23], which considers the statistics of singularity strengths of multiple local scale invariance, since in most cases a specific description of the system must be abandoned in favor of probabilistic ones. This scale invariance is normally a consequence of some hierarchical organization of the underlying process [18]. So in this way moments and cumulants are studied to get information and characterize scale invariance or scale affinity, or to detect them if this is not the case.

The organization of the paper is as follows. In Sec. II the model is briefly described. Section III is devoted to the description of the computational methods used in this paper. The results of our work are presented and discussed in Sec. IV, and finally we end the paper by summarizing our conclusions in Sec. V.

II. MODEL

In this paper we study the vibrational dynamics of the isomerizing molecular system LiCN/LiNC using classical mechanics. This is a floppy molecule with a large amplitude motion in the bending Li-CN coordinate which couples very efficiently with the corresponding stretching mode, and a high frequency mode associated with the stiff C≡N chemical bond. Accordingly, the CN mode can be considered from the practical point of view separated from the rest of molecular motions, and a reduced 2dof model, in which the C≡N distance is held frozen at its equilibrium value of $r_e = 2.186$ a.u., can be used to adequately describe its dynamics. The floppy bending motion samples big regions of the potential energy surface, and then chaos sets in at very moderate values of the excitation energy.

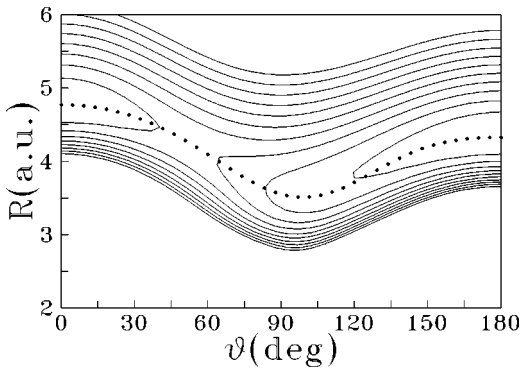

FIG. 1. Contour plot of the potential energy surface of LiNC/LiCN. The minimum energy path connecting the two potential wells is shown superimposed as a dotted line.

The classical vibrational ($J=0$) Hamiltonian is given by

$$H = \frac{P_R^2}{2\mu_{\text{Li-CN}}} + \frac{1}{2}\left(\frac{1}{\mu_{\text{Li-CN}}R^2} + \frac{1}{\mu_{\text{C-N}}r_e^2}\right)P_\theta^2 + V(R,\theta), \tag{2}$$

where R is the distance from the Li atom to the center of mass of the CN fragment, θ is the angle between the N-C and R vectors, and P_R and P_θ are the corresponding conjugate momenta.

The potential energy surface, $V(R,\theta)$, shown in Fig. 1 in the form of a contour plot, has been taken from the literature [25], and consists of a ten term expansion in Legendre polynomials,

$$V(R,\theta) = \sum_{\lambda=0}^{9} V_\lambda(R) P_\lambda(\cos\theta), \tag{3}$$

fitted to *ab initio* calculations. As can be observed, it has two potential wells corresponding to the stable linear isomers: Li-NC ($\theta = 180°$) and Li-CN ($\theta = 0°$). The minimum energy path, $R_e(\theta)$, connecting these two isomers has also been plotted in the figure.

III. COMPUTATIONAL METHODS

A. Dynamical study

The dynamics of the system is studied using classical trajectories calculated by numerical integration of the Hamilton

equations of motion corresponding to Eq. (2), using a hybrid Gear algoritm [26]. The phase space structure is visualized by computing a Poincaré SOS taking the sectioning plane lying along the minimum energy path, $R_e(\theta)$ [27]. Owing to the fact that the sectioning coordinate does not correspond to a constant value of any of the canonical coordinates used to define the Hamiltonian function, the Poincaré SOS so defined does not have the (important) property of being an area-preserving map. In order to solve this problem we make the following canonical transformation [28]:

$$\rho = R - R_e(\theta),$$

$$\psi = \theta,$$

$$P_\rho = P_R,$$

$$P_\psi = P_\theta + \left(\frac{dR_e}{d\theta}\right) P_\rho. \tag{4}$$

With these new coordinates we can now define the Poincaré SOS as $\rho = 0$ with P_ρ chosen as one of the roots obtained by substituting Eq. (4) in Eq. (2), which corresponds to mapping the trajectories of the system in the (ψ, P_ψ) plane.

B. Frequency analysis (FA)

For each trajectory the complex functions

$$f_R(t) = R(t) + iP_R(t),$$

$$f_\theta(t) = \theta(t) + iP_\theta(t), \tag{5}$$

defined in the time interval $[-T, T]$, were analyzed by carrying out FA as described below.

The $f(t)$ functions can be written as

$$f(t) = \sum_{n=-\infty}^{\infty} a_n e^{i\pi nt/T}, \tag{6}$$

where the coefficients a_n are the projection of $f(t)$ on the Fourier basis elements, $e_n = \exp(\mathrm{i}\pi nt/T)$,

$$a_n = \langle e^{i\pi nt/T} | f(t) \rangle, \tag{7}$$

where $\langle\,|\,\rangle$ denotes a complex symmetric inner product, and not a complex conjugation as usually done in quantum mechanics. The frequencies calculated by the Fourier transform are determined within a precision of π/T [29]. To go beyond this approximation one must resort to a different basis set, using a better suited set of exponents. For this purpose we will use the prescription developed by Laskar [15]. The first frequency, ν_1, is chosen to maximize the scalar product

$$\phi_1(\nu) = \langle e^{i\nu_1 t} | f(t) \rangle, \tag{8}$$

starting from an initial guess calculated with a standard fast Fourier transform (FFT) method [29]. The other frequencies are obtained in a similar way by searching for those values of ν_n maximizing

$$\phi_n(\nu) = \langle e^{i\nu_n t} | f_{n-1}(t) \rangle, \tag{9}$$

where the $f_{n-1}(t)$ functions are obtained by eliminating from $f(t)$ the contributions from the previously determined frequencies, $\{\nu_1, \nu_2, \ldots, \nu_{n-1}\}$.

Since the basis set formed by the elements $e^{\mathrm{i}\nu_n t}$ is not orthogonal, it is necessary at this point to carry out a Gram-Schmidt orthonormalization procedure. After that, one obtains $f(t)$ as

$$f(t) = \sum_n b_n e^{i\nu_n t}. \tag{10}$$

In this way very accurate fundamental frequencies can be determined.

When performing the scalar products a Hanning window filter,

$$\chi(t) = 1 + \cos(\pi t/T), \tag{11}$$

is used to accelerate convergence.

C. Multifractal analysis (MFA)

The results obtained from the frequency analysis are studied in terms of the percentage of frequencies distributed in different initial conditions (θ angle) . Thus, the measure p_i in this system is defined by the fraction of the frequencies in an angle class "i." The support of this measure is the set of real numbers corresponding to θ values from θ_0 to θ_f degrees. Thus, p_i can be interpreted as the probability of finding frequencies of a certain value within the θ interval i being $p(\theta_0, \theta_f] = 1$ (or 100%).

The structure of this probability measure p on the segment $(\theta_0, \theta_f]$ may be defined by the scaling relationship

$$p \propto \delta^\alpha \quad \text{as} \quad \delta \to 0, \tag{12}$$

where the scaling exponent α is the so-called Lipschitz-Hölder exponent, and δ is the length of the subintervals in which the total segment is divided.

In general the concentration of frequencies varies widely over the interval $(\theta_0, \theta_f]$ and a different behavior is observed in different spatial positions. Thus, a spectrum of values of α, that correspond to different spatial positions, can be defined. In fact, every measure p_i may be characterized by α_i such that $p_i \propto \delta^{\alpha_i}$. Hence the singularity exponent α is a function of the position i, many sites i may share the same exponents when a regular covering of size δ is chosen. Therefore, let $N(\alpha, \delta)$ be the number of sites i that share the same measure p_i, which presents the following scaling relationship:

$$N(\alpha, \delta) \propto \delta^{-f(\alpha)} \quad \text{as} \quad \delta \to 0, \tag{13}$$

where the $f(\alpha)$ singularity spectrum describes the statistical distribution of the Hölder exponent α, or in other words gives information of how often specific values α of the singularity strengths occur [22].

This indicates that the density of segments $[\rho(\alpha)]$ of length δ with the Hölder exponent value α in the range $(\alpha,\alpha+d\alpha)$ is approximately $\delta^{-f(\alpha)}$, due to

$$N(\alpha,\delta)=\rho(\alpha)d\alpha. \tag{14}$$

There are several methods to calculate the $f(\alpha)$ singularity spectrum. The method we have used is based on a quantity called the partition function $(\chi(q,\delta))$, introduced by the method of the moments [30], as

$$(\chi(q,\delta))=\sum_{i=1}^{n(\delta)} p_i^q, \tag{15}$$

where $n(\delta)$ is the number of subintervals of size δ in the largest interval $(\theta_0,\theta_f]$, and q is the weight or moment of the measure. This partition function depends on the scale δ and on the exponent q as it can be observed in Eq. (15). A log-log plot of a self-similar measure $(\chi(q,\delta))$ vs δ at various values for q will give

$$(\chi(q,\delta))\sim\delta^{-\tau(q)}, \tag{16}$$

where $\tau(q)$ is the qth mass exponent [22] and sometimes is called the Renyi exponent [23]. We can express $\tau(q)$ as

$$\tau(q)=-\lim_{\delta\to 0}\frac{\log(\chi(q,\delta))}{\log\delta}. \tag{17}$$

Then the generalized dimension D_q can be introduced by the following scaling relationship [23]:

$$D_q=\lim_{\delta\to 0}\frac{\log(\chi(q,\delta))}{(q-1)\log\delta}, \tag{18}$$

and therefore

$$\tau(q)=(q-1)D_q. \tag{19}$$

On the other hand, the partition function can be expressed as

$$\chi(q,\delta)=\int N(\alpha,\delta)p_\alpha^q d\alpha, \tag{20}$$

where p_α is the measure, its Lipschitz-Hölder exponent is α (i.e., $p_\alpha\propto\delta^\alpha$), and this relationship can be expressed as [17]

$$\chi(q,\delta)=\int \rho(\alpha)\delta^{q\alpha-f(\alpha)}d\alpha. \tag{21}$$

Namely, if we cover the support of the measure p with segments of length δ, the number of such segments that scale like δ^α, for a given α, behaves like $N(\alpha,\delta)\propto\delta^{-f(\alpha)}$. In the limit $\delta\to 0$, the sum of $p(q,\delta)$ is dominated by the term $\delta^{\min_\alpha(q\alpha-f(\alpha))}$. Then $\tau(q)$ can be expressed as

$$\tau(q)=\min_\alpha[q\alpha-f(\alpha)]. \tag{22}$$

Thus, $\tau(q)$ is obtained by Legendre transforming the $f(\alpha)$. When $f(\alpha)$and $\tau(q)$ are smooth functions we can express [17]

$$\alpha(q)=-\frac{d}{dq}\tau(q),$$

$$f(\alpha(q))=q\alpha(q)-\tau(q). \tag{23}$$

A multifractal measure will show an $f(\alpha)$ curve with a parabolic shape. Several meaningful parameters can be obtained from the spectrum. Two of them are α_{max} and α_{min} which give the amplitude of the convex function $(f(\alpha))$ [24], defined for the case when $f(\alpha)=0$, as $\alpha_{max}-\alpha_{min}$.

In this work a direct determination of the $f(\alpha)$, as suggested by Chhabra and Jensen [31], is preferable. The following relationships were applied to calculate $f(q)$ and $\alpha(q)$ from the normalized measure:

$$f(q)=\lim_{\delta\to 0}\frac{\sum_{i=0}^{n(\delta)} p_i(q,\delta)\log[p_i(q,\delta)]}{\log\delta}, \tag{24}$$

$$\alpha(q)=\lim_{\delta\to 0}\frac{\sum_{i=0}^{n(\delta)} p_i(q,\delta)\log[p_i(1,\delta)]}{\log\delta}. \tag{25}$$

$f(\alpha)$ is then obtained by plotting $f(q)$ vs $\alpha(q)$ for each value of q.

In this case the value of q varies from -8 to $+8$ with an increment of 0.5, and the number of points $n(\delta)$ used in each regression line, for a fixed q, was always 13.

IV. RESULTS

In Fig. 2 we present the composite SOS for LiNC/LiCN at nine different vibrational energies, chosen as the eigenenergies corresponding to quantum levels number 20 to 100 in increments of 10 [28]. The first four energies [2(a)–2(d)] are above that of the least stable isomer, Li-CN, but below the potential barrier for the isomerization process LiNC⇌LiCN, so that motion is classically possible in both potential wells, depending on the initial conditions, but they are unconnected. The other energies, [2(e)–2(i)], are above that barrier, with the possibility of trajectories in which the Li atom orbits around the CN fragment, exchanging its position between the two wells (isomerization process). As can be seen in the figures the dynamics in the Li-CN isomer well (higher in energy) is always more regular than that corresponding to the Li-NC (lower in energy). Actually, it is only after level number 50 [Plot 2(d)] that a small band of stochasticity in the border of the available phase space appear. Also, two promi-

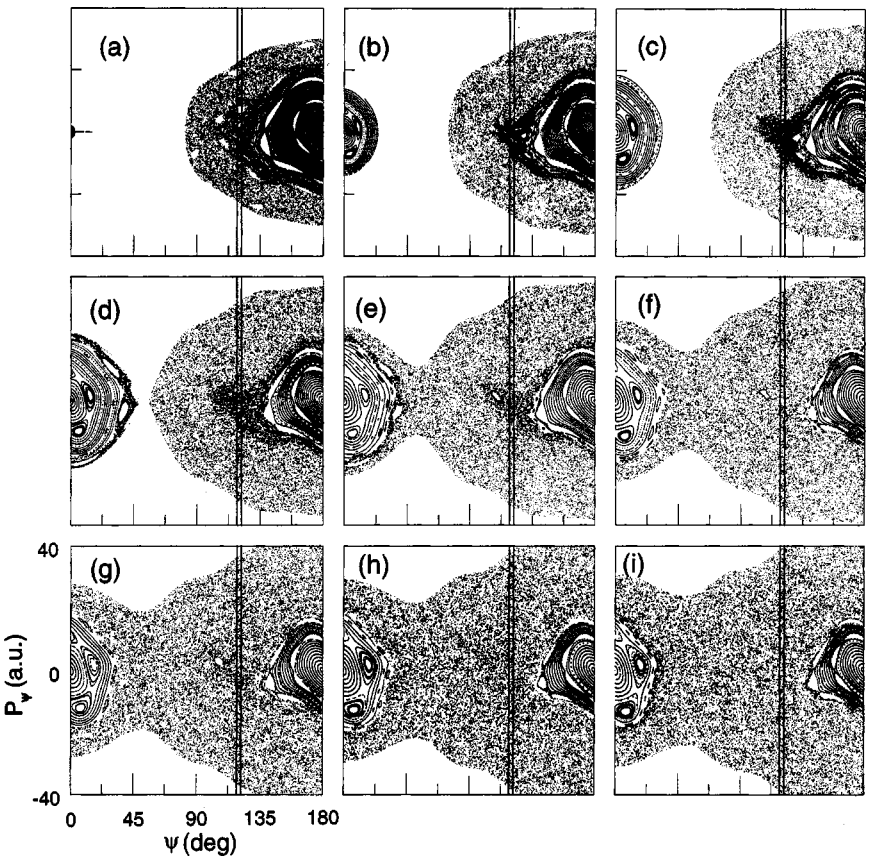

FIG. 2. Classical Poincaré surface of section for the LiNC/LiCN isomerization system at different values of the vibrational energy: 2299.0 cm^{-1}, 2759.2 cm^{-1}, 3122.3 cm^{-1}, 3441.4 cm^{-1}, 3702.7 cm^{-1}, 3953.7 cm^{-1}, 4167.2 cm^{-1}, 4386.4 cm^{-1}, 4596.0 cm^{-1}, which correspond to the quantum levels $N=20$, 30, 40, 50, 60, 70, 80, 90, 100, (a)–(i), respectively.

nent resonances of order 1:4 and 1:6, respectively, are visible. On the other hand, the dynamics in the LiNC well ($\theta = 180°$) present a mixed character, in which chaotic and regular motions coexist. Moreover, the fraction of the chaotic part grows with energy, in agreement with the statement of the KAM theorem. The location and extent of the different possible resonances are also visible. It is also important to notice a conspicuous accumulation of chaotic points in plots 2(b)–2(e), around the edge of the regular region centered on the LiNC isomer. This accumulation is an indication of the difficulty that the trajectories have in getting in and out of this region, being the signature of the existence of a very intact cantorus [32], acting as an effective dynamical bottleneck separating the chaotic region in two parts. It can also be inferred from the figure that the effect of this cantorus tends to dissapear as energy increases [see plots 2(f)–2(i)].

To obtain a more quantitative information of these structures, we have carried out a FA at the same energies considered above for trajectories starting on the SOS with $P_\psi = 0$ at different values of the initial angle. The results for the frequency ratios, ν_R/ν_θ, are shown versus ψ_0 in Fig. 3. All resulting plots consist of two very different parts. One very regular, formed by smooth, well behaved lines, corresponding to the regular regions in the SOS around the potential isomer wells. These lines are continuous, except for a few points associated with small discontinuities arising from low order resonances [14]. The second part in the ν_R/ν_ψ curve appears in the central part of the plot and corresponds to the chaotic part of the SOS. It is formed by a seemingly irregular cloud of scattered points. However, as discussed in Ref. [14], this part is not completely unstructured. For one thing, the dispersion of frequencies in the region inside the existing cantorus is much larger, indicating that the behavior in this region is very chaotic. On the other hand, the ergodic dynamics in the outer part appears to be much milder, with a big accumulation of points around the value $\nu_R/\nu_\theta = 8$ (this resonance also plays a very important role in the quantum dynamics of this system, as reported in Ref. [33]).

As discussed above, the dynamics at the higher energies [plots 3(e)–3(i)] takes place in all range of angles, being the two isomer wells connected. Here the cantorus is very destroyed, and the difference in behavior inside and outside it is not very significative. Also, it should be noticed that as energy increases, the 1:8 resonance begins to lose importance, and the dynamics is less constrained; as a consequence the variations in ν_R/ν_ψ are bigger.

Let us examine now in more detail the part of the chaotic region in which the frequencies of the system vary more widely. For that purpose, we have concentrated in a small area of phase space in the inner part of the cantorus, carrying out a FA on 10^4 trajectories starting at initial angles, ψ_0, between the two vertical lines drawn in Figs. 2 and 3 (remember the condition $P_{\psi,0}=0$ when locating the region in Fig. 2). The trajectories have been followed for 9000 time intervals (22 ps). The corresponding frequency ratios as a function of the angle class, $i=\psi_0/180°$ (see Sec. III C) are presented in Fig. 4. To make the figure clear we have represented only those points with $\nu_R/\nu_\theta \leqslant 30$. Several accumulations are noticed. For the state $N=20$ [plot 4(a)], frequencies appear at $\nu_R/\nu_\theta = 10$, 11, 12. Notice that this result is partly

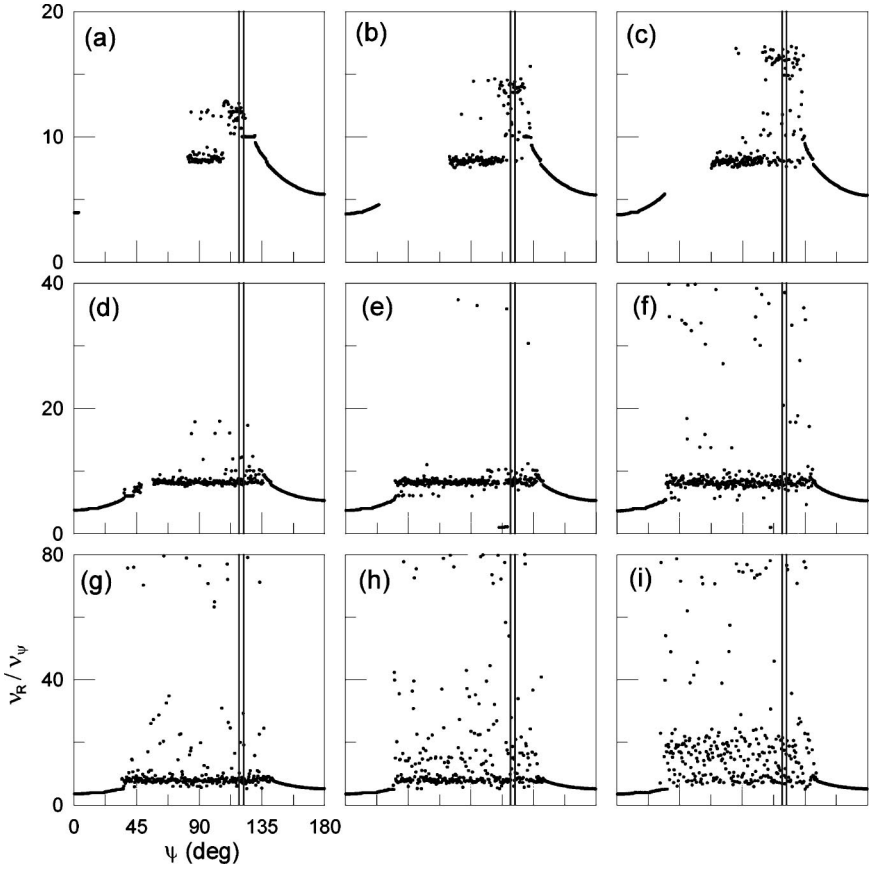

FIG. 3. The frequency ratio as a function of the initial angle for an ensemble of trajectories started along $P_\psi = 0$ cut on the SOS for LiNC/LiCN at the same energies as in Fig. 2.

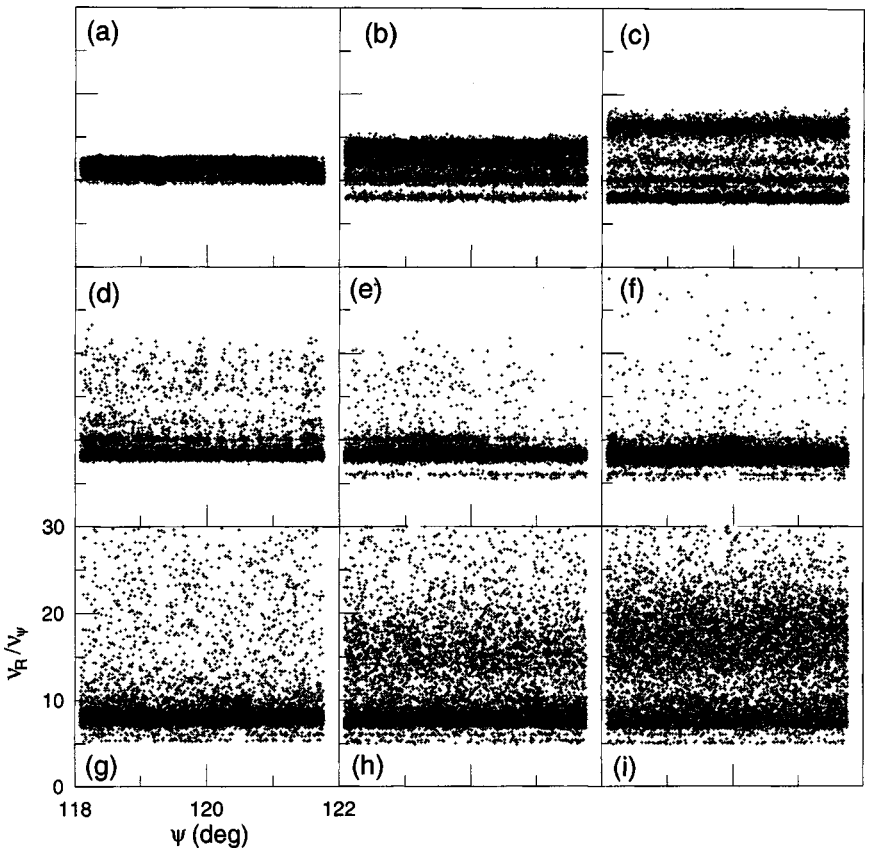

FIG. 4. The frequency ratio of the irregular region selected in Fig. 3 for the same nine energies as considered in the mentioned figure. Plots (a)–(i) correspond to the vibrational energies indicated in Fig. 2.

due to the election of the initial angles, and the resulting values are not representative of the whole chaotic region at this energy. However, this does not represent a problem for our purposes, since we are only interested in this part of the paper in the quantitative characterization of the tori destruction. For $N=30$ and 40 [plots 4(b) and 4(c)] the range opens up to 8, 10, 12, and 14 and 8, 10, 12, and 16, respectively. For $N=50$ [plot 4(d)] the interval reduces considerably to 8 and 10, plus a multitude of scattered points. For $N=60$ and 70 [plots 4(e) and 4(f)], that correspond to energies above the isomerization barrier, the picture is more or less the same, with the appearance of a new accumulation around the 1:6 resonance. Finally, for $N=80$–100 (plots g-i) the only visible accumulation takes place around $\nu_R/\nu_\theta=8$, and the ''sticking'' power of this resonance seems to decrease with the excitation energy.

To make this visual description more quantitative, we have performed a MFA of these point distributions. The multifractal spectra of the frequency distributions are shown in Fig. 5, where for the sake of clarity the results are presented in two plots, corresponding to states with energies below and above the isomerization barrier, respectively. The shape of $f(\alpha)$ shows clearly that we are in the presence of a multifractal at all energies considered. Similar results have also been reported in the literature for the analysis of the scaling structure of power spectra in dynamical systems [34]. The variation of the calculated slopes depending on the number of points used in the regression line was studied. The slope value varied when the number of points were less than 10, and for a regression line of 10 points and more the differences were statistically nonsignificant. Based on this analysis and taking into account the demanding computational time of the calculations, the number of points selected to calculate the slope values of the regression lines were 13.

Another point worth commenting on is the convexity of the f versus α curve, which is not symmetric with respect to its maximum. This can be ascertained by comparing the values of $f(\alpha)$ for $q=8$ and $q=-8$. The appearance of lower values in the positive side (left side of the curve) of the q's correlates with a bigger influence of the highest values of the FM in the spectral complexity. On the contrary, lower values of $f(\alpha)$ for negative q's (right side of the curve) indicate a higher influence of the lowest values in the complexity. In our case, almost all results correspond to the first option, except for $N=30$ and 100 in Fig. 5(A), and $N=24$, 28 and 30 in Fig. 5(B), where the lower values of FM are given more complexity to the structure of the spectra. The effect can also be appreciated by careful examination of points in Fig. 4.

The variations in the complexity of the spectra can be ascertained [24] by plotting their amplitudes, $\Delta\alpha=\alpha_{\max}-\alpha_{\min}$, obtained at different energies versus the vibrational energy. The corresponding results are shown in Fig. 6, where it can be seen that, although the overall tendency is towards complexity, this behavior is not smooth and the curve presents some oscillations. The changes in $\Delta\alpha$ are consistent with the distributions of the frequency ratios and the normalized measure p at each energy. Then, for the energies corresponding to states 20 to 40 the value of $\Delta\alpha$ increases, which

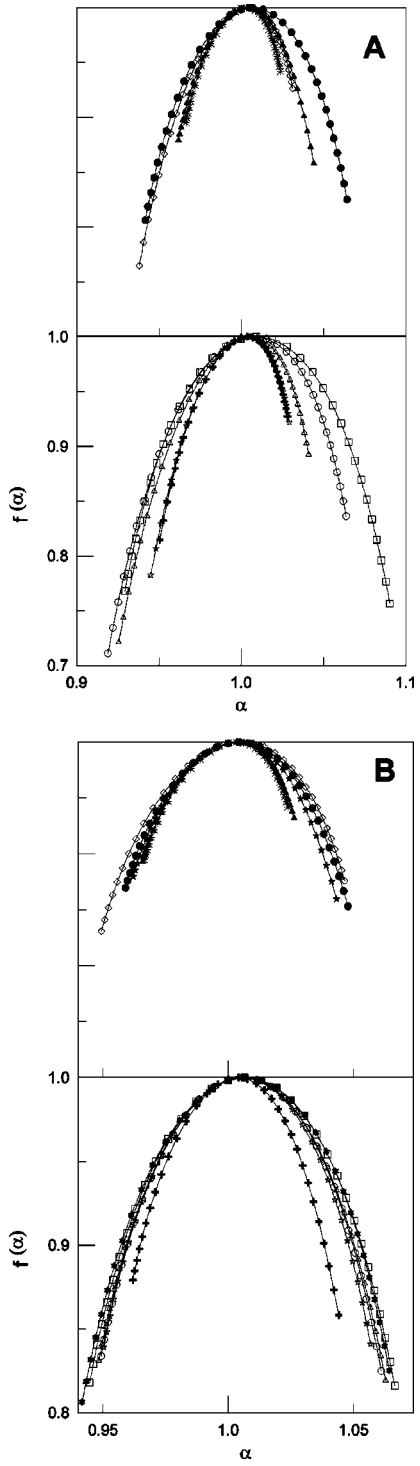

FIG. 5. Multifractal spectra $f(\alpha)$ of the frequency distribution for LiNC/LiCN (part A) for energies below (top) and above (bottom) the isomerization barrier. The different curves correspond to the energies of the states $N=20$ (*), 30 (▲), 40 (●), 50 (◇); (bottom) 60 (+), 70 (⋆), 80 (△), 90 (○), and 100 (□). Part B correspond to the energies 2299.0 cm^{-1}, 2431.7 cm^{-1}, 2549.2 cm^{-1}, 2630.5 cm^{-1}, 2744.3 cm^{-1}, 2759.2 cm^{-1}, 2852.9 cm^{-1}, 2930.6 cm^{-1}, 2981.4 cm^{-1}, 3094.8 cm^{-1}, 3122.3 cm^{-1}, associated with the following states: (top) $N=20$ (*), 22 (▲), 24 (●), 26 (◇), 28 (⋆); (bottom) 30 (+), 32 (⋆), 34 (△), 36 (○), 38 (□) and 40 (⋆).

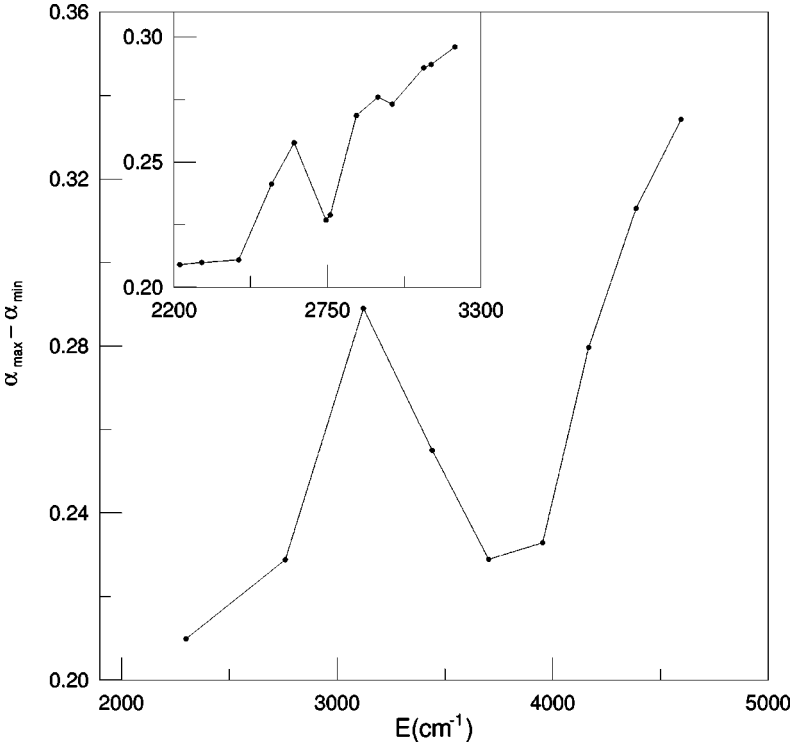

FIG. 6. Multifractal amplitude $\Delta\alpha=\alpha_{\max}-\alpha_{\min}$ corresponding to Fig. 5 as function of the vibrational energy. The inset corresponds to the result of Fig. 5(B)

is a reflection of the fact that the distribution [see Figs. 4(a)–4(c)] divides in several clouds of points centered around different values of ν_R/ν_θ. After that, for states 50, 60, and 70, the tendency reverses, getting $\Delta\alpha$ for $N=60$ the same low value as obtained for $N=30$. In this process the complexity of the spectrum decreases as a consequence of the accumulation of points around the value $\nu_R/\nu_\theta=8$. Finally, for states above the 80th the increasing tendency is regained and the range of α values spreads out; this is induced by an increment in the number of points with higher values of the frequency ratio which increases the complexity of the spectra.

To conclude this section, let us examine now in more detail the results corresponding to the increasing part of $\Delta\alpha$ between the energies corresponding to $N=20$ and 40 at intervals of two energy levels. For this purpose the multifractal spectra of the frequency distributions at this range of energies have been obtained and are shown in Fig. 5(B). In it we can observe a generally similar behavior that was obtained for the whole range of energies [Fig. 5(A)]. From these results the corresponding amplitudes, $\Delta\alpha=\alpha_{\max}-\alpha_{\min}$, have been also obtained and plotted versus the vibrational energy in the inset of Fig. 6.

Again, although in the overall behavior the spectral complexity increases with the excitation energy, this tendency is not monotonous, and several up and downs are appreciated in the curve. What is more remarkable is that these oscillations are similar to those exhibited by the complete curve at a greater scale, thus suggesting the possibility that the whole curve may be self-similar.

V. CONCLUSION

In this paper we have presented and analyzed in detail the phase space structure of the chaotic region closer to the regular tori for the molecular vibration of the isomerizing system LiNC/LiCN. The system is described by a realistic 2dof model, in which the potential energy surface is taken from *ab initio* calculations existing in the literature. The interaction potential corresponds to a highly anharmonic double well separated by a moderate energy barrier.

The classical results have been analyzed using both the traditional procedure of constructing Poincaré surfaces of section, and the method of frequency analysis. This latter method has revealed the existence of two different regimes in the chaotic dynamics of the system under study, one inside an existing cantorus acting as an efficient dynamical barrier, and the other outside the surface defined by this invariant structure. Moreover, at low energies the chaotic character of the trajectories has been found to be stronger in the inner part of the cantori than outside it. Also, this difference tends to decrease with energy, since the cantorus get more destroyed. In the outside region the chaotic dynamics of the LiNC/LiCN appear to be strongly influenced by a 1:8 resonance between the stretching Li-NC and the bending modes. At higher energies another resonance, namely the 1:6, starts to be important. The corresponding POs not only govern the classical motion of the system, but also play an important role in the associated quantum mechanics. Accordingly, many states are found to be scarred by these simple classical structures.

The KAM theorem provides an explanation for the mechanism of destruction of tori in the region inside the above-mentioned cantori. By analyzing the frequency map results obtained in a small area of this region, we have shown in this paper the existence of a multifractal structure whose complexity varies with the total vibrational energy of the system. This structure is related to the proportion of intact new cantori and the more destroyed ones. The multifractal scaling has been also discussed.

Finally, one point worth considering is that of the limits of validity of the conclusions drawn in this work. For example, to what extent the multifractal structures described here are a general phenomenon and the destruction of tori is governed by some kind of renormalization properties [35]. In this respect, we are currently extending our studies to open (scattering) chaotic systems [36], in which the possibility of different types (exponential versus potential law) of escaping times behavior exists as a function of the hyperbolic or nonhyperbolic character of the underlying chaotic dynamics [37]. This will be the subject of a future paper.

ACKNOWLEDGMENT

This work was supported in part by DGES (Spain) under Contract No. BFM2000–347.

[1] S. Wiggins, *Chaotic Transport in Dynamical Systems* (Springer-Verlag, New York, 1992).
[2] J. Simons and J. Nichols, *Quantum Mechanics in Chemistry* (Oxford University Press, Oxford, 1997).
[3] A.J. Lichtenberg and M.A. Lieberman, *Regular and Chaotic Dynamics* (Springer-Verlag, New York, 1992).
[4] R. de la Llave, in *Smooth Ergodic Theory and its Applications*, edited by A. Katok, R. de la Llave, Y. Pesin, and H. Weiss, Proceedings of Symposia in Pure Math. (AMS, Providence, 2001), Vol. 69, pp. 175–292.
[5] P. Cvitanovic, B. Shraiman, and B. Söderberg, Phys. Scr. **32**, 263 (1985); P. Veerman, Physica D **29**, 191 (1987).
[6] B.B. Mandelbrot, *The Fractal Geometry of Nature* (Freeman, San Francisco, 1983).
[7] G. Radons, T. Geisel, and J. Rubner, Adv. Chem. Phys. **73**, 891 (1988).
[8] See, for example, C.B. Olds, *Continued Fractions* (Random House, New York, 1963).
[9] J.M. Greene, J. Math. Phys. **20**, 1183 (1979); G. Schmidt, Phys. Rev. A **22**, 2849 (1980); I. Dana, Phys. Rev. Lett. **64**, 2339 (1990).
[10] G. Schmidt and J. Bialek, Physica D **5**, 397 (1982).
[11] E. Lorenz, *The Essence of Chaos* (UCL Press, London, 1995).
[12] *Hamiltonian Systems with Three or More Degrees of Freedom*, edited by C. Simó (Kluwer, Dordrecht, 2000).
[13] V.I. Arnold and A. Avez, *Ergodic Problems of Classical Mechanics* (Addison-Wesley, Reading, MA, 1989).
[14] J.C. Losada, J.M. Estebaranz, R.M. Benito, and F. Borondo, J. Chem. Phys. **108**, 63 (1998).
[15] J. Laskar, C. Froeschle, and A. Celletti, Physica D **56**, 253 (1992); J. Laskar, *ibid.* **67**, 257 (1993); H.S. Dumas and J. Laskar, Phys. Rev. Lett. **70**, 2975 (1993).
[16] J. Laskar, F. Joutel, and P. Robutel, Nature (London) **361**, 615 (1993).
[17] K. Falconer, *Fractal Geometry* (Wiley, Chichester, England, 1990).
[18] C. Meneveau and K.R. Sreenivasan, Phys. Rev. Lett. **59**, 1424 (1987).
[19] R.V. Solé and S.C. Manrubia, J. Theor. Biol. **173**, 31 (1995).
[20] H. Grout, A.M. Tarquis, and M. Wiesner, Environ. Sci. Technol. **32**, 1176 (1998).
[21] T. Vicsek, Physica A **168**, 490 (1990).
[22] H. Feder, *Fractals* (Plenum Press, New York, 1988).
[23] R. Holley and E.C. Waymire, Ann. Appl. Probab. **2**, 819 (1992).
[24] J.G. Hou, Wang Yan, Xia Rui, Zhu Xiaoguang, Wang Haiqian, and Z.Q. Wu, Phys. Rev. E **58**, 2213 (1998).
[25] R. Essers, J. Tennyson, and P.E.S. Wormer, Chem. Phys. Lett. **89**, 223 (1982).
[26] C.W. Gear, SIAM (Soc. Ind. Appl. Math.) J. Numer. Anal. **2B**, 69 (1964).
[27] F. Borondo and R.M. Benito, in *Frontiers of Chemical Physics*, edited by E. Yurtsever (Kluwer, Dordrecht, 1995).
[28] R.M. Benito, F. Borondo, J.-H. Kim, B.G. Sumpter, and G.S. Ezra, Chem. Phys. Lett. **161**, 60 (1989).
[29] W.H. Press, B.P. Flannery, S.A. Teukolsky, and W.T. Vetterling, *Numerical Recipes* (Cambridge University Press, Cambridge, 1986).
[30] C.J.G. Evertsz and B.B. Mandelbrot, in *Chaos and Fractals: New Frontiers of Science*, edited by H. Peitgen, H. Jurgens, and D. Saupe (Springer-Verlag, New York, 1992), pp. 921–953.
[31] A. Chhabra and R.V. Jensen, Phys. Rev. Lett. **62**, 1327 (1989).
[32] R.S. McKay, J.D. Meiss, and I.C. Percival, Physica D **13**, 55 (1984); P. Bensimon and L.P. Kadanoff, *ibid.* **13**, 82 (1984).
[33] F.J. Arranz, F. Borondo, and R.M. Benito, Phys. Rev. Lett. **80**, 944 (1998).
[34] M. Giona, L. Marelli, and P. Piccirilli, J. Non-Cryst. Solids **131-133**, 71 (1991).
[35] S. Kim and S. Ostlund, Phys. Rev. Lett. **55**, 1165 (1985); J.D. Meiss, Phys. Rev. A **34**, 2375 (1986).
[36] C. Jung and T.H. Seligman, Phys. Rep. **285**, 77 (1997); R. Guantes, F. Borondo, and S. Miret-Artés, Phys. Rev. E **56**, 378 (1997).
[37] R. Guantes, S. Miret-Artés, and F. Borondo, Phys. Rev. B **63**, 235401 (2001).